Chapter 1

Synthesis and Luminescent Properties of Silicon Nanocrystals

Antonio Coyopol-Solis, Tomás Díaz-Becerril,
Godofredo García-Salgado,
Santiago A. Cabañas-Tay,
Liliana Palacios-Huerta and
Alfredo Morales-Sánchez

Additional information is available at the end of the chapter

http://dx.doi.org/10.5772/intechopen.74286

Abstract

Nowadays, study of silicon-based visible light-emitting devices has increased due to large-scale microelectronic integration. Since then different physical and chemical processes have been performed to convert bulk silicon (Si) into a light-emitting material. From discovery of Photoluminescence (PL) in porous Silicon by Canham, a new field of research was opened in optical properties of the Si nanocrystals (Si-NCs) embedded in a dielectric matrix, such as SRO (silicon-rich oxide) and SRN (silicon-rich nitride). In this respect, SRO films obtained by sputtering technique have proved to be an option for light-emitting capacitors (LECs). For the synthesis of SRO films, growth parameters should be considered; Si-excess, growth temperature and annealing temperature. Such parameters affect generation of radiative defects, distribution of Si-NCs and luminescent properties. In this chapter, we report synthesis, structural and luminescent properties of SRO monolayers and SRO/SiO_2 multilayers (MLs) obtained by sputtering technique modifying Si-excess, thickness and thermal treatments.

Keywords: SRO monolayers, silicon nanocrystals, sputtering, multilayers

1. Introduction

The use of photonic signals instead of electrons to transmit information through an electronic circuit is an actual challenge. Unfortunately, it is well known that bulk silicon (Si) is an indirect bandgap semiconductor, making it an inefficient light emitter. Therefore, great efforts have

been taken to obtain highly luminescent Si-based materials in order to get Si-based photonic devices, especially a light-emitting device [1–3]. Such circumstances have led to explore new options for converting silicon into a luminescent material. Si-NCs embedded in a dielectric material as silicon-rich oxide (SRO) or silicon-rich nitride (SRN) show a prominent photoluminescence (PL) emission in red and blue-green region, respectively [4, 5]. Thus, SRO films have been considered as promising candidates for potential applications in Si-based optoelectronic devices, and their fully compatibility with the complementary metal-oxide-semiconductor (CMOS) processes. At present, different techniques or methods have been employed to produce SRO films or SRO/SiO_2 MLs [6–13]. In such structures, the SRO-thickness, Si-excess and annealing temperature are parameters that promote the formation of Si-NCs and radiative defects, affecting the optical and electrical properties of SRO monolayers or SRO/SiO_2 ML.

In this chapter, results about of Si-NCs embedded at SRO monolayer and SRO/SiO_2 MLs deposited by the RF Co-sputtering method as a function of Si-excess (5.2–14.3 at.%) and modulating the SRO-thickness layer (2.5–7.5 nm) of MLs are shown. Both, SRO monolayers and SRO/SiO_2 MLs have a broad emission band in the orange-red region (1.45–2.3 eV). Nevertheless, the SRO/SiO_2 MLs emit a stronger PL intensity compared with SRO monolayers. The most intense PL emission is observed in MLs when the SRO-thickness is 5 nm, and with the highest Si-excess (14.3 at.%), which is important for the design of electroluminescent devices with low threshold voltage. Although multilayer structures with good control in crystal size have been studied [14], in this chapter optical and structural properties are analyzed in detail. Furthermore a comprehensive study of synthesis of Si-NCs in SRO and SRO/SiO_2 MLs as a function of Si-excess (5.2–14.3 at.%) and annealing temperature is presented.

2. Experimental procedure

In this chapter, structural and optical properties of co-sputtered SRO monolayers and SRO/SiO_2 MLs are obtained and studied as a function of the annealing temperature and the change in the Si-excess. Both structures were deposited by the co-sputtering of Si (2“, purity of 99.999 %) and SiO_2 (2“, purity of 99.99%) targets using a Torr International magnetron sputtering system (13.56 MHz). Both structures were deposited on p-type (100) Si wafers with resistivity of 2–5 Ω-cm. Before deposition, Si substrates were cleaned in ultrasonic bath with acetone, ethanol, and deionized water successively. After being dried with nitrogen, the substrates were immediately loaded into the chamber of the sputtering system. Once a base pressure of ~1×10^{-6} Torr is achieved, Ar flow of 60 sccm is introduced into the chamber at a working pressure of 2.4 mTorr.

The SRO monolayers were deposited by the simultaneous co-sputtering of Si and fused quartz (SiO_2) targets. The Si-excess content in SRO monolayers was modified by changing the RF power applied to the Si-target (PSi) from 40 to 80 W maintaining constant the RF power applied to the SiO_2 target (P_{SiO_2} = 100 W). Thus, RF-power densities to the Si-target (PD_{Si}) were applied; 1.97, 2.47, 2.96, 3.45, and 3.94 W/cm^2 to obtain 4.4, 5.2, 10.2, 14.3, and 16.9 at.% of Si-excesses, respectively (**Table 1**). On the other hand, the RF-power density applied to the

Sample	Sample topology	Si-excess (at.%)	≈Thickness (nm)	
			As-deposited	Annealed
A	SRO monolayer	5.2	108	90
B	SRO monolayer	10.2	82	70
C	SRO monolayer	14.3	90	76

Table 1. Thickness and Si-excess obtained for SRO monolayers.

Sample	Sample topology	Si-excess (at.%)	Total ≈ Thickness (nm)	
			As-deposited	Annealed
1A	~2.5 nm-SRO/~6 nm-SiO_2		107	105
2A	~5 nm-SRO/~6 nm-SiO_2	**5.2**	135	127
3A	~7.5 nm-SRO/~6 nm-SiO_2		165	150
1B	~2.5 nm-SRO/~6 nm-SiO_2		99	103
2B	~5 nm-SRO/~6 nm-SiO_2	**10.2**	130	120
3B	~7.5 nm-SRO/~6 nm-SiO_2		170	152
1C	~2.5 nm-SRO/~6 nm-SiO_2		107	102
2C	~5 nm-SRO/~6 nm-SiO_2	**14.3**	140	124
3C	~7.5 nm-SRO/~6 nm-SiO_2		168	154

Table 2. SRO and SiO_2 thickness and Si-excess in the SRO/SiO_2 multilayer structures.

SiO_2 target (PD_{SiO_2}) was 5.09 W/cm^2. For SRO/SiO_2 MLs, SRO interlayers with the same Si-excess that SRO monolayers were used. First, a SiO_2 layer was deposited onto the silicon substrate followed by a SRO film to obtain a SRO/SiO_2 bi-layer. Ten periods of SRO/SiO_2 bi-layers were deposited with an additional (upper) SiO_2 film (10 nm) to avoid oxidization during high temperature annealing. Each SiO_2 layer was about 6 nm in thick while the SRO layer thickness was modified from 2.5 to 7.5 nm (see **Table 2**).

All samples were deposited at 100°C. However, Si-NCs in SRO monolayers and SRO/SiO_2 MLs were produce by thermal annealing in a conventional tube furnace between 900 and 1200°C in N_2 environment for 2 h. Thickness of the films was measured by reflectance using a Filmetrics F20UV equipment. The chemical compositions and Si-excess of samples were analyzed by a Thermo Scientific X-ray photoelectron spectroscopy (XPS) Escalab 250Xi equipment. The Si oxide phase was studied by Fourier transform Infra-red (FTIR) spectroscopy using a Bruker Vector 22 spectrometer in the range 400–4000 cm^{-1}. The PL emission spectra were measured with a Horiba Fluoromax 3 system. The samples were excited using a 300 (4.13 eV) nm radiation and the PL emission signal was collected from 400 to 900 nm (1.37–3.1 eV) with a resolution of 1 nm.

3. Deposition rate Si and SiO_2 films

The first step to synthesize silicon nanocrystals embedded in SRO films by Co-sputtering is to consider the deposition rate of Si and SiO_2 films. Such procedure allows to obtain RF powers appropriate to Si and SiO_2 targets and silicon content suitable for SRO films. Some experimental studies report RF powers applied to the Si higher than SiO_2 target [15, 16]. However, it is known that the deposition rate of SiO_2 is low (0.1Å/sec) and high silicon content could be present in SRO films if the deposition rate of Si is much higher than the SiO_2 film. This effect is shown in **Figure 1**; where Si and SiO_2 films were individually deposited for 1200 s using Si and SiO_2 targets, respectively.

Figure 1 shows the deposition rate and thickness of Si and SiO_2 films as function of the RF-power density (PD) applied to Si and SiO_2 targets. It can be observed that the deposition rate for SiO_2 is lower (0.15 Å/s) at 100 W while that Si films (0.12 Å/s) at 50 W, where similar thickness (~16–18 nm) is deposited with a $PD_{Si} = 2.47$ W/cm² for a Si film and $PD_{SiO_2} = 5.09$ W/cm² for a SiO_2 film. Therefore, to ensure Si-excess similar to the reported by other techniques [17–21], SRO films were deposited considering RF-power densities between 1.97 and 3.94 W/cm² applied to the Si-target and a PD_{SiO_2} constant of 5.09 W/cm². Selected the appropriate power densities, SRO monolayers and SRO/SiO_2 ML were deposited at 100°C and annealed at 1100°C.

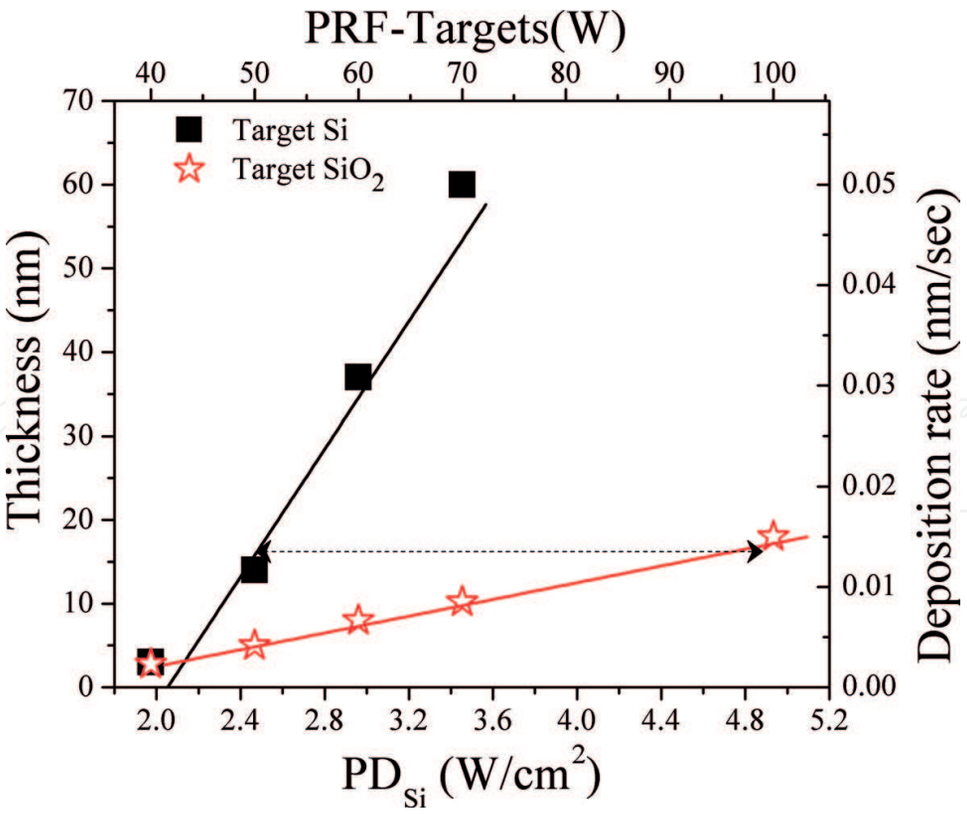

Figure 1. Deposition rate and thickness of Si and SiO_2 films as function of the RF-power density. From Coyopol et al. [25].

http://dx.doi.org/10.5772/intechopen.74286

4. Atomic composition and XPS-Si2p of SRO monolayers and SRO/SiO_2 multilayers

4.1. SRO monolayers

The optimization of sub-stoichiometric silicon-rich oxide (SRO) from precise control of Si content in SRO films is an important parameter to tune the electrical and optical properties of luminescent and photovoltaic devices. In this regard, it has been reported that there might be an optimal Si-excess to find an efficient photoluminescence (PL) emission [18, 19]. The PL quantum yield of SRO films ($1.4 < x < 1.9$) annealed at 1100°C, increase significantly for a Si content x = 1.8 (2.5 at.% of Si-excess) [18]. For this Si-excess, Si-NCs are not detected by HRTEM, however intense emission in red region was observed. It has been suggested that for a medium Si-excess (<9 at.%), oxygen-related defects, such as Si=O (nonbridged

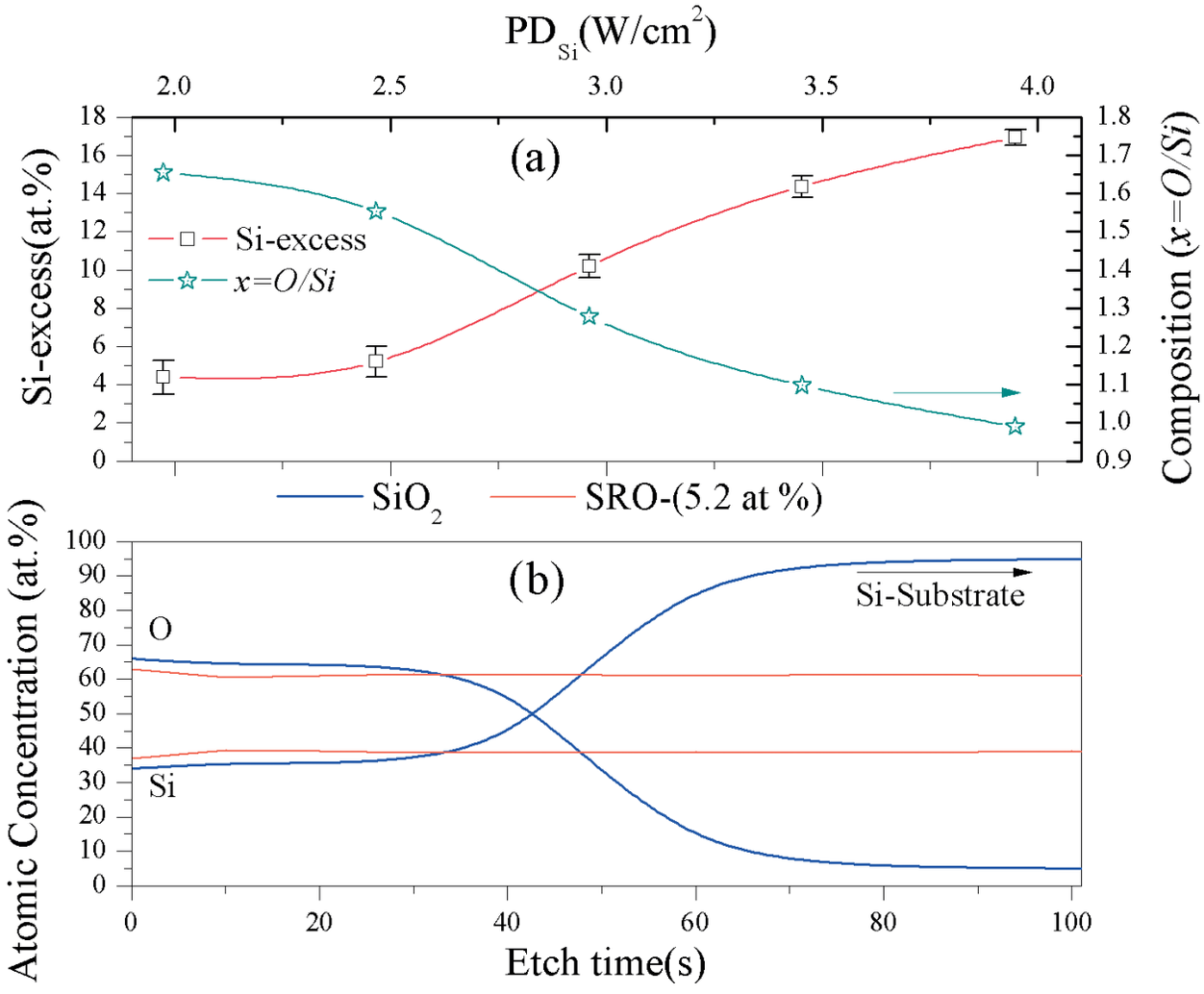

Figure 2. (a) Si-excess and x in SRO as a function of the power density applied to Si-target. (b) XPS in-depth profile of SRO monolayer with 5.2 at.% of Si-excess respect to SiO_2 film.

oxygen passivation) and/or ultra-small oxidize Si-NCs (diameters <2 nm) are the most optically actives for promote an intense emission in red region (1.5 eV). Thus, a considerable Si-excess (>10 at.%) in SRO films is not necessary to obtain a maximum PL emission.

In this chapter Si-excess between 4.4 and 16.9 at.% are reported. In order to know the composition (x = O/Si) and Si-excess of SRO monolayers and SRO/SiO_2 multilayers, XPS measurements in-depth profile were performed. In **Figure 2b**, the analysis in-depth profile of an SRO film with 5.2 at.% of Si-excess compared to a SiO_2 film is shown. It can be seen that silicon content in SRO film increase respect to SiO_2 film. The atomic concentration of Si content in SRO film was ≈38.5 at.% respect to the SiO_2 film with an atomic concentration of ≈33.33 at.%. Such effect demonstrates Si-excess in SRO monolayers. For all SRO monolayers Si-excess increases from 4.4 to 16.9 at.% as the power density of Si-target rise from 1.97 to 3.94 W/cm^2, respectively (see **Figure 2a**). Where, Si-excess of 4.4, 5.2, 10.2, 14.3, and 16.9 at.% were found for PD_{Si} values of 1.97, 2.47, 2.96, 3.45 and 3.94 W/cm^2, respectively.

The presence of Si-excess in SRO films is also detected by the oxidation states of Si obtained from Si2p-XPS data. This fact is suggested on the basis of the intermediate oxidation states detected in the Si2p-XPS spectra. According to Si-excess measured by XPS, five oxidation states were detected in samples, before and after annealing. For example for a SRO monolayer with 5.2 at.%, peaks located around 99.6 eV, 100.5, 101.5, 102.5 and 103.5 eV were found

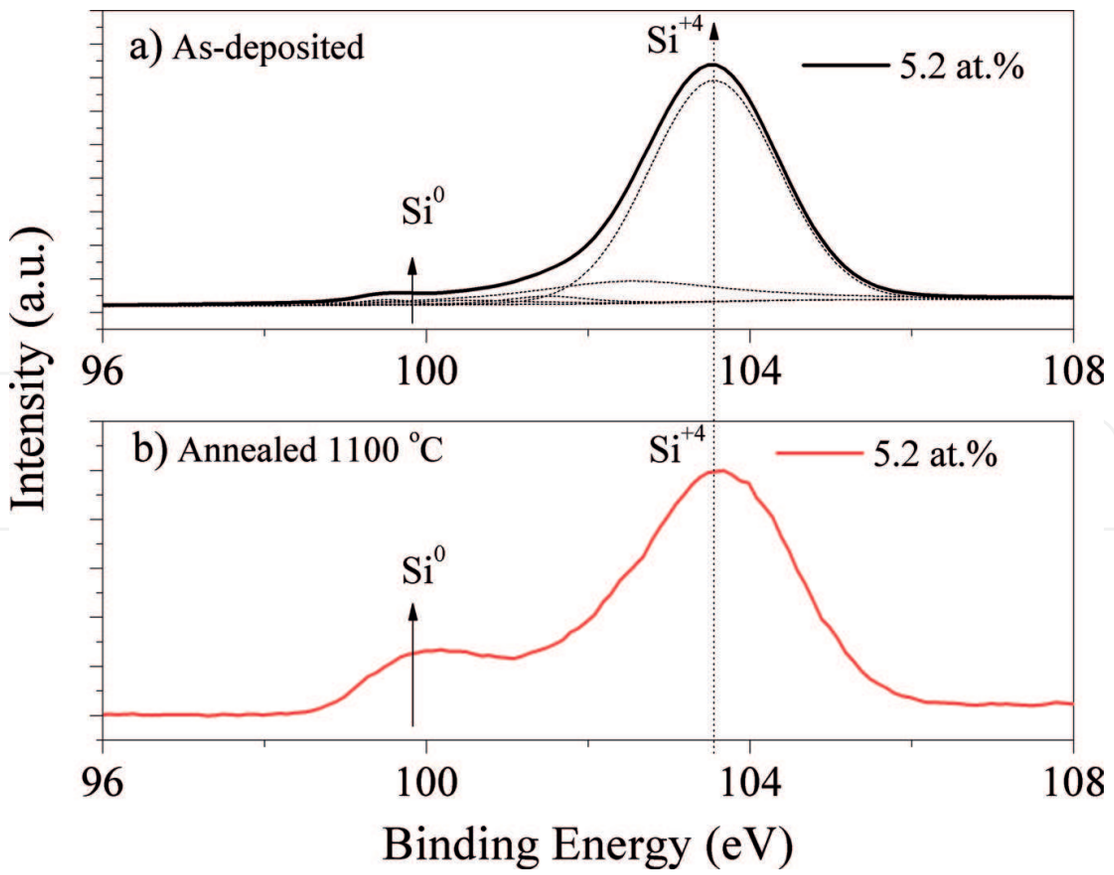

Figure 3. Si2p-XPS peaks of SRO monolayer (5.2 at.% of Si-excess) (a) as-deposited and (b) annealed at 1100°C.

(**Figure 3a**). The aforementioned peaks correspond to the Si^0 (elemental Si), Si^{+1} (Si_2O), Si^{+2} (SiO), Si^{+3} (Si_2O_3) and Si^{+4} (SiO_2) oxidation states, respectively [22, 23]. The contributions of the intermediate Si peaks (Si^{+1}, Si^{+2}, Si^{+3}) corresponding to the suboxide phases become smaller when the SRO films are thermally annealed at 1100°C, while Si^{+4} peak for SiO_2 and Si^0 peak for elemental Si becomes dominant, especially the intensity of Si^0 peak increases (**Figure 3b**), explaining the Si-SiO_2 phase separation and Si-NCs formation after annealing, as shown by similar results found by Chen et al. [24].

4.2. SRO/SiO_2 MLs

For the design of SRO/SiO_2 ML structures, SRO layers with the same Si-excess that monolayers were used. In **Figure 4a**, the composition in-depth profile for an as-deposited SRO/SiO_2 MLs with 5 nm-thick SRO layer corresponding to 5.2 at.% and 10.2 at.% of Si-excess is shown. As we can see, different changes in atomic concentration (x) are observed corresponding to different SRO-SiO_2 interfaces as the etch time increases. A better contrast between SRO and SiO_2 stoichiometry is observed when the Si-excess and SRO-thickness is increased to 14.3 at.% and 7.5 nm, respectively (sample 3C, before and after annealing), as observed in **Figure 4b**. A densification in thickness is observed in this multilayer after thermal annealing and it is attributed to a microstructural reordering in SRO layers.

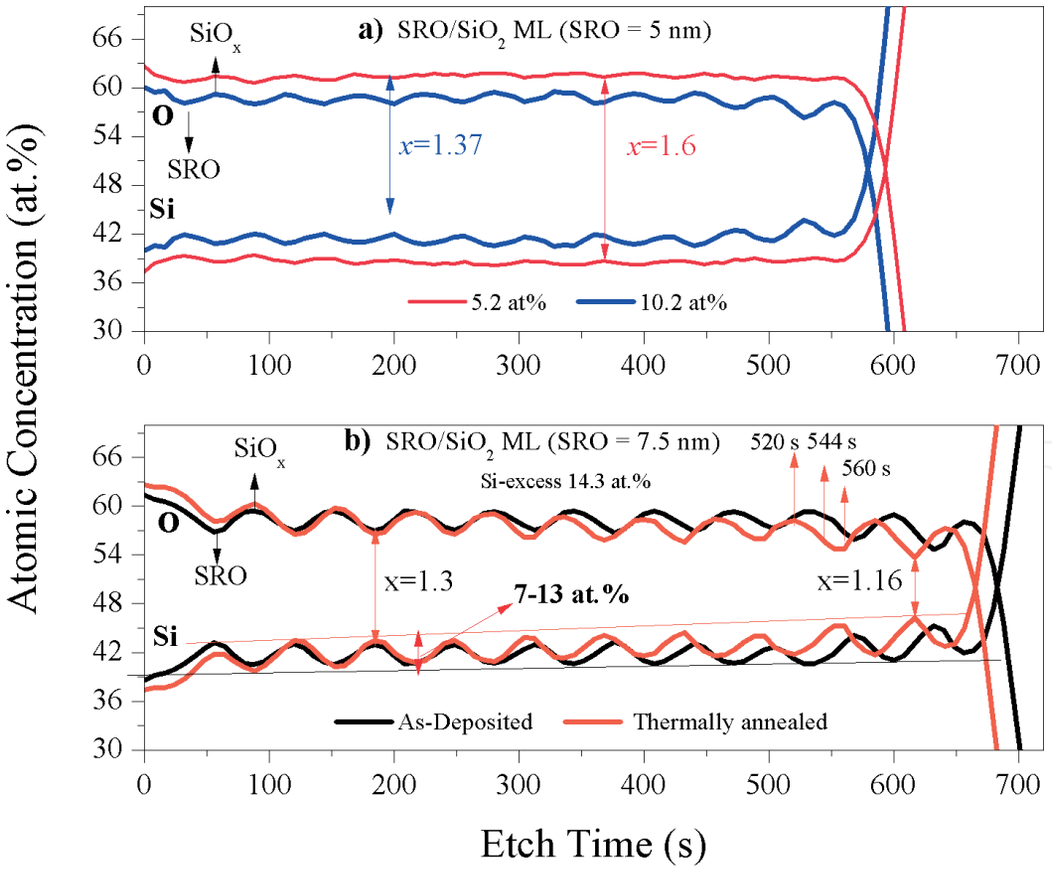

Figure 4. XPS in-depth profile of (a) as-deposited multilayer (SRO-5 nm) with 5.2 at.%, 10.2 at.% of Si-excess and (b) multilayer (SRO-7.5 nm) with 14.3 at.%-before and after thermal annealing (1100°C). From Coyopol et al. [28].

The atomic concentrations (x) obtained in multilayers as-deposited (x = 1.37, x = 1.6) are near to SRO monolayers (x = 1.3, x = 1.5). Such difference or reduction of atomic concentration could be caused by the etch time performed by XPS. A reduction of the atomic concentration (x) in sample 3C by effect annealing is observed (**Figure 4b**), even this effect being more noticeable near the substrate (x = 1.3 → x = 1.16). In this way, it is likely that a re-diffusion of Si atoms between SRO-SiO_x interfaces as well as within SRO layers after thermal treatment is performed. Such annealing, promotes crystallization of Si clusters and Si-NCs formation between SRO-SiO_x interfaces [25–27]. The Si-excess or Si clusters within of multiple SRO layers were detected from Si2p-XPS analysis. For this study, sample 3C was analyzed specifically in the etch time range of 520–560 s (see **Figure 4b**), specifically in critical points; SiOx layer (520 s), near the SRO-SiOx interfaces (544 s) and SRO layer (560 s) as is shown in **Figure 5**.

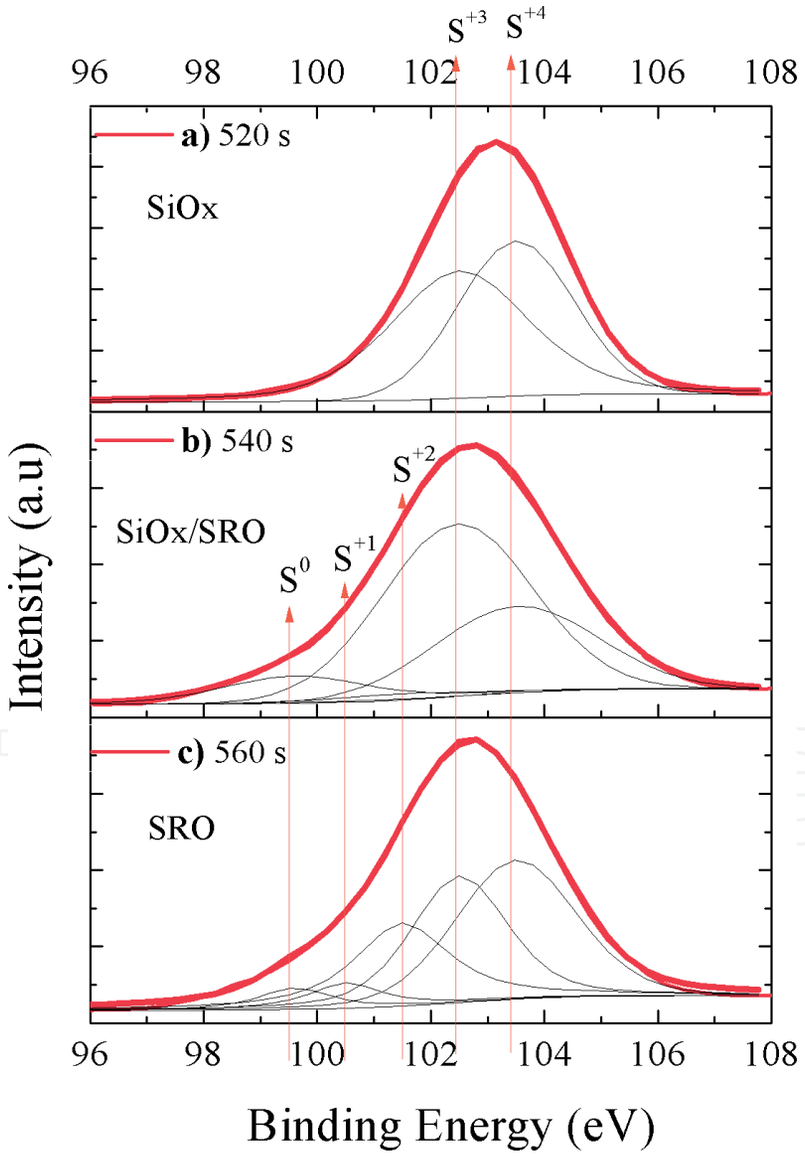

Figure 5. Si2p-XPS peaks of multilayer (SRO-7.5 nm) with 14.3 at.%- thermal annealing (1100°C) with a etch time range analysis at (a) 520 s (SiO_x layer), (b) 544 s (SRO-SiO_x interfaces) and (c) 560 s (SRO layer).

It can be observed that for etch time at 560 (SRO) and 540 s (SRO-SiO_x), five oxidation states were detected, located around 99.6 eV, 100.5, 101.5, 102.5 and 103.5 eV (**Figure 5b** and **c**). For Si2p-XPS analysis in 520 s (SiO_x), the oxidation state Si^0 was not detected (**Figure 5a**), only oxidation states Si^{+3} and Si^{+4} were detected, so that Si atoms diffusion is unlikely in this region. Thereby, for an etch time at 544 and 560 s, five oxidation states were perfectly adjusted, even the Si^0 state is greater in 544 s, which could be tentatively edges SRO-SiO_x interface. Therefore Si-diffusion is likely even in the SRO-SiO_x interfaces and SRO nanolayers. This study evidences crystallization of silicon clusters after annealing and formation of Si-NCs in the SRO-SiO_2 interfaces and the SRO nanolayers by Si atoms diffusion. This effect was demonstrated before by HRTEM measurements [25, 28].

5. FTIR and effect annealing of SRO monolayers and SRO/SiO_2 MLS

5.1. SRO monolayer

The nature of the chemical bonds and the phase separation of Si and SiO_2 of SRO monolayers before and after thermal annealing are studied by FTIR. **Figure 6a**, shows FTIR spectrum of as-deposited SRO monolayers with 5.2, 10.2 and 14.3 at.% of Si-excess. As shown in **Figure 6a**, three characteristic rocking, bending, and asymmetric stretching Si-O-Si vibrational modes of SiO_2 are

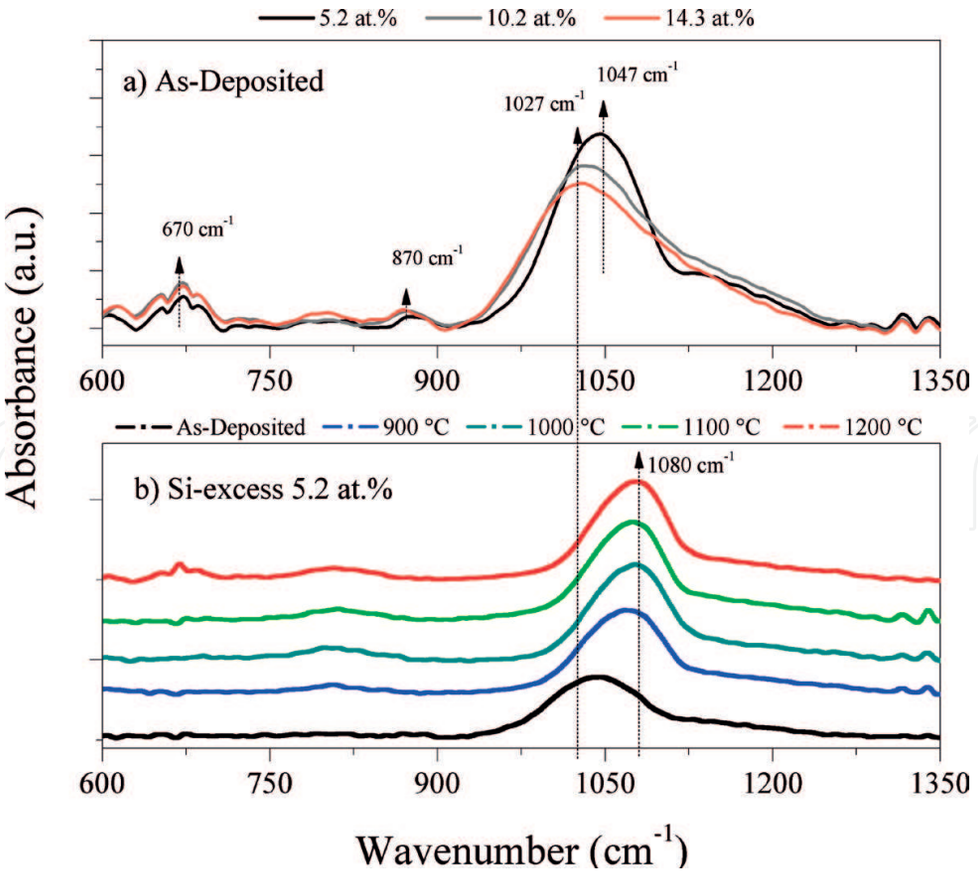

Figure 6. FTIR spectra of SRO monolayers (a) As-deposited and (b) Thermally annealed at 900°C, 1000°C, 1100°C, 1200°C.

observed at around 446–450, 800–872, and 1026–1040 cm^{-1}, respectively [29]. The Si-O-Si stretching band shifts toward low wavenumbers (1047–1027 cm^{-1}) as the silicon content increases (from 5.2 to 14.3 at.%) in as-deposited monolayers. An additional IR band of low intensity is observed around 880 cm^{-1}. Such vibrational mode disappears when samples are thermally annealed, indicating a rearrangement of the SiO_x network due to a diffusion of Si atoms, which promotes Si-SiO_x phase separation and the formation of Si-NCs in SRO layers [25–27]. **Figure 6b**, shows the effect of annealing between 900 and 1100°C on SRO monolayer of 5.2 at.% of Si-excess, where the disappearance of band located around 880 cm^{-1} is observed. Likewise, a phase separation and Si-NCs formation in SRO monolayers is corroborated by the shift observed in the Si-O-Si stretching band position (1047–1080 cm^{-1}) after thermal annealing [25, 27]. It can be seen that for an annealing above about 1000°C, stretching peak appears at 1080 cm^{-1}. Such effect means that temperatures above 1000°C are sufficient for Si-SiO_x phase separation and Si-NCs formation in the SRO monolayers. It is worth mentioning that an annealing temperature of 1100°C by 2 h provided better results in the structural and optical properties [25, 28].

5.2. SRO/SiO_2 multilayers

Figure 7 shows the evolution of the FTIR spectra in the range of 900–1280 cm^{-1} for SRO/SiO_2 MLs (14.3 at.% of Si-excess) with a SRO-thickness of 2.5 (sample 1C), 5 (sample 2C), and

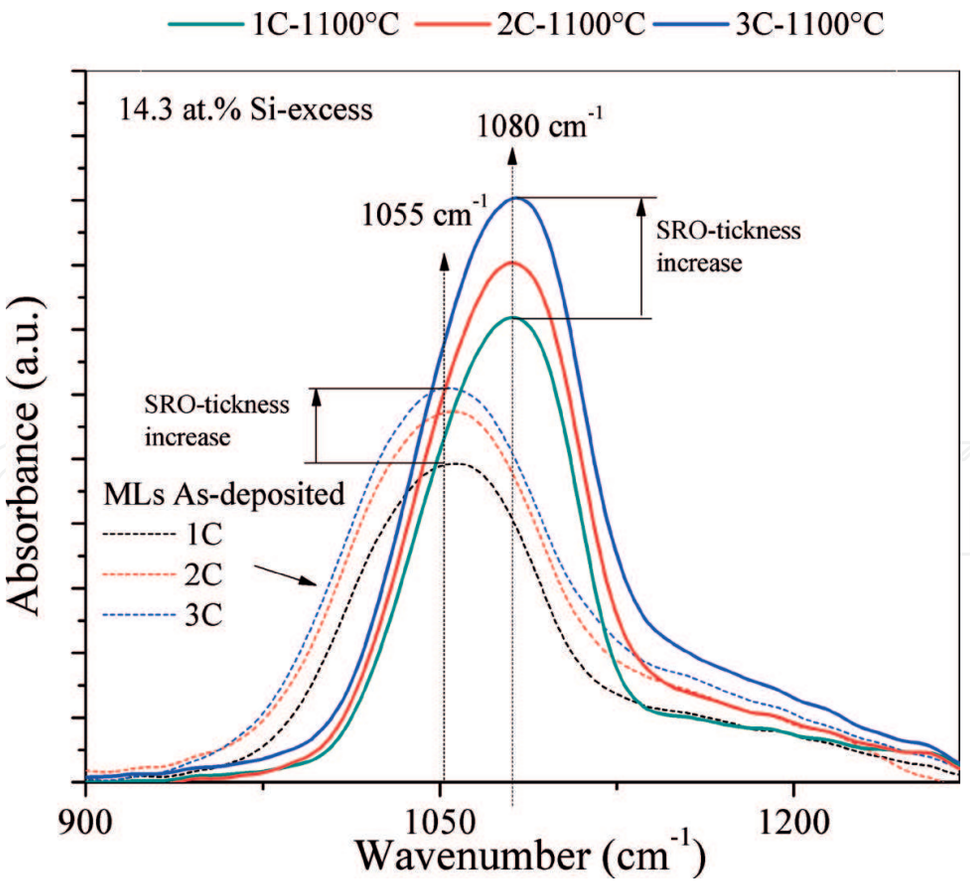

Figure 7. FTIR spectra of SRO/SiO_2 MLs as function of SRO-thickness (2.5–7.5 nm) of as-deposited and thermally annealed at 1100°C.

7.5 nm (sample 3C), before and after thermal annealing (1100°C). For MLs as-deposited, the stretching peak position remains at 1055 cm^{-1} due to the same Si-excess, 14.3 at.%. However, intensity of the stretching peak is modified as thickness of SRO intermediate layers increase (2.5–7.5 nm), which is to be expected since the thickness of the MLs increases (**Table 2**) and the number Si-O-Si bonds of these molecules increases. The shift in the Si-O-Si stretching band was also observed from 1055 to 1080 cm^{-1} after the thermal annealing. This effect, again, indicates a phase separation (Si-SiO_x) and therefore the Si-NCs formation within the SRO-bulk layers and possibly in the SRO-SiO_2 interfaces. By other hand, all SRO/SiO_2 MLs exhibited narrower Si-O-Si stretching bands respect to the SRO monolayers. Such effect at SRO/SiO_2 MLs can be related to a higher structural order in the SRO matrix due to a compressive stress in Si-NCs [30]. In MLs structures, the compressive stress exerted on the Si-NCs is higher unlike monolayers, where the structural order of the SRO matrix is the lowest resulting in a broad IR spectrum. Thus, it is likely that smaller nanocrystals (diameters <3 nm) must be confined in the SRO/SiO_2 MLs due to the high stress.

6. PL of SRO monolayers and SRO/SiO_2 MLs

6.1. SRO Monolayers

Figure 8a shows the PL spectra of SRO monolayers thermally annealed at 1100°C for different Si-excess. It can be seen that when Si-excess increases of 4.4–16.9 at.%, the PL emission intensity is modified. The emission intensity of this band (red region) increases considerably for the SRO monolayer with 5.2 at.% thermally annealed at 1100°C. It has been reported that SRO films deposited by LPCVD or MBE with medium Si-excess (~2.5–5 at.%) produces an efficient PL emission, however Si-NCs have not been observed [17–21]. In our case, Si-NCs were observed from a Si-excess of 5.2 at.% (x = 1.54), as it was shown in images HRTEM [25]. The PL emission in SRO films with 14.3 and 16.9 at.% is still perceptible, however is weak due to the high silicon content, even close to SiO film (x = 1). In this case, PL intensity decreases due to an increase of Si-NCs size, larger to the Bohr radius or to annihilation of radiative centers. Regarding to the PL emission observed in sample whit 4.4 of Si-excess (PD_{Si} = 1.97). A moderate emission is observed in the **Figure 8a**. According to the low concentration in this sample (x = 1.64), such emission is attributed to the formation of ultra-small oxidized Si-NCs as well as some point defects [18, 19]. It has been suggested that for a medium Si-excess (<9 at.%), oxygen-related defects, such as Si=O (Nonbridged oxygen passivation) and/or ultra-small oxidized Si-NCs (diameters <2 nm) are the most optically active centers that promote an intense emission in red region (~1.5–1.7 eV). Accordingly, Si-NCs with diameters larger than 3 nm (Si-excess >10 at.%) are not direct light-emitting centers [18, 19]. Thus, a considerable Si-excess (>10 at.%) in SRO films is not necessary to obtain a maximum PL emission.

The effect of the annealing temperature (900–1200°C) on the PL properties of the SRO monolayers also was analyzed (**Figure 8b**). The best PL emission intensity was obtained for the sample with Si-excess of 5.2 at.% (x = 1.54) and annealed at 1100°C. Thus, for the other annealing temperatures, PL intensity decreases, so a temperature of 1100° C is ideal for obtaining a maximum PL emission in SRO monolayers obtained by RF Co-Sputtering.

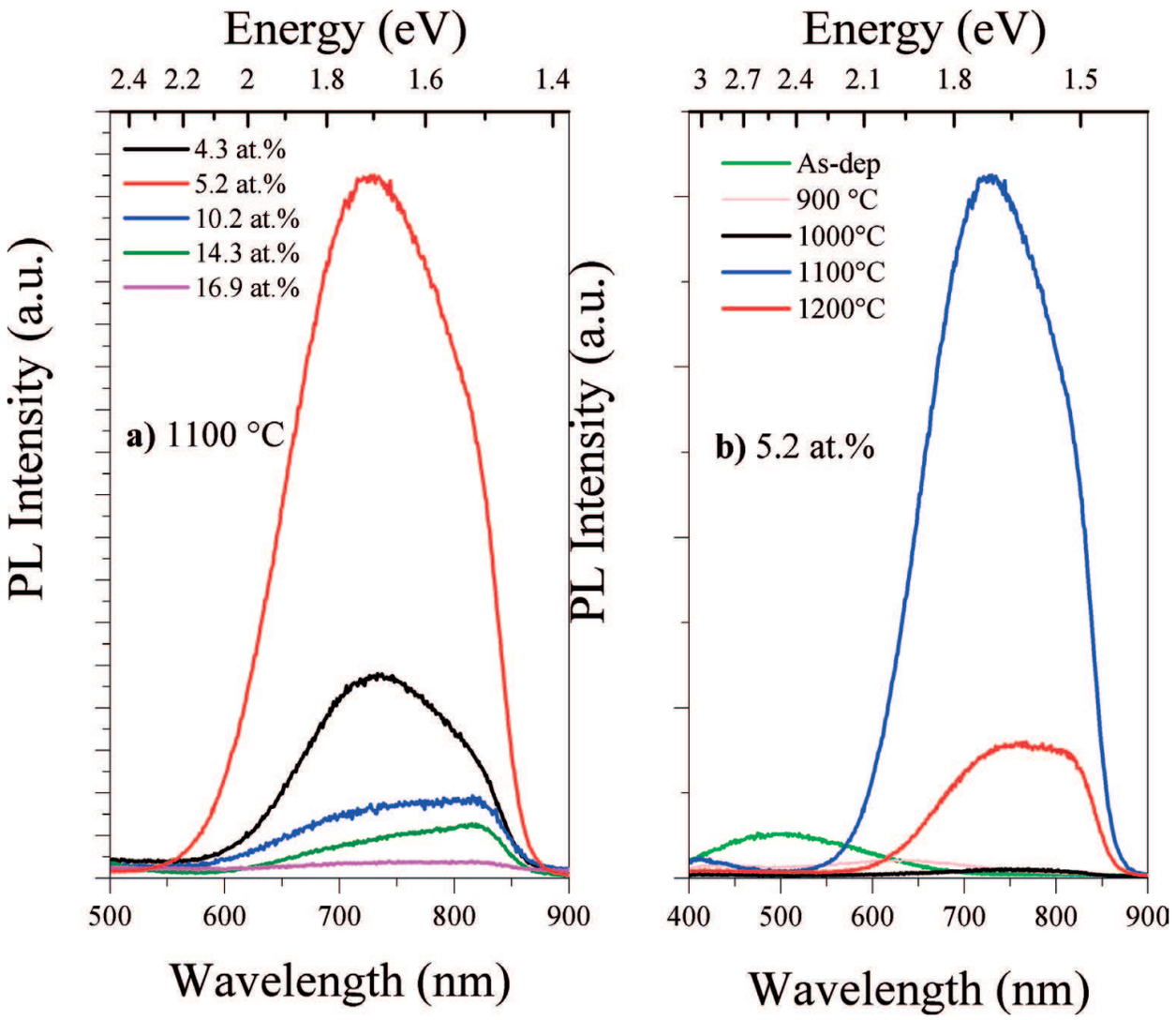

Figure 8. PL spectra of SRO monolayers (a) thermally annealed at 1100°C for different Si-excess and (b) annealed at different temperatures with 5.2 at.% of Si-excess.

6.2. SRO/SiO_2 MLs

The maximum PL emission in the SRO monolayers is obtained with a Si-excess between 5.2 and 14.3 at.% and heat treated at 1100° C. In this way for the design of the structures MLs, Si-excess of the same order was used. Both, monolayers and multilayers, emit an intense and broad emission band in the red-orange region (1.45–2.1 eV). **Figure 9b** and **a**, shows, respectively, the PL spectra of thermally annealed SRO monolayers and SRO/SiO_2 MLs with a SRO-thickness of 5 nm with different Si-excesses [28]. In this case it was found that the MLs with a thickness of 5 nm in the SRO layer, has a maximum of PL emission independent of the Si-excess. For this, an analysis of PL intensities was made considering the ratio of maximum peaks of intensities of the SRO/SiO_2 MLs and SRO monolayer. Such analysis to determine the MLs with greater emission as function of Si-excess and SRO-thickness layer. The ratio of emission intensities was calculated taking the maximum PL intensity of each peak (~1.72, ~1.6 and ~1.52 eV) that form the PL spectrum of each SRO/SiO_2 ML (I_{PL} ML) divided by the maximum PL intensity of SRO monolayers (I_{PL} Mono) located at the same energy [28]. So, the

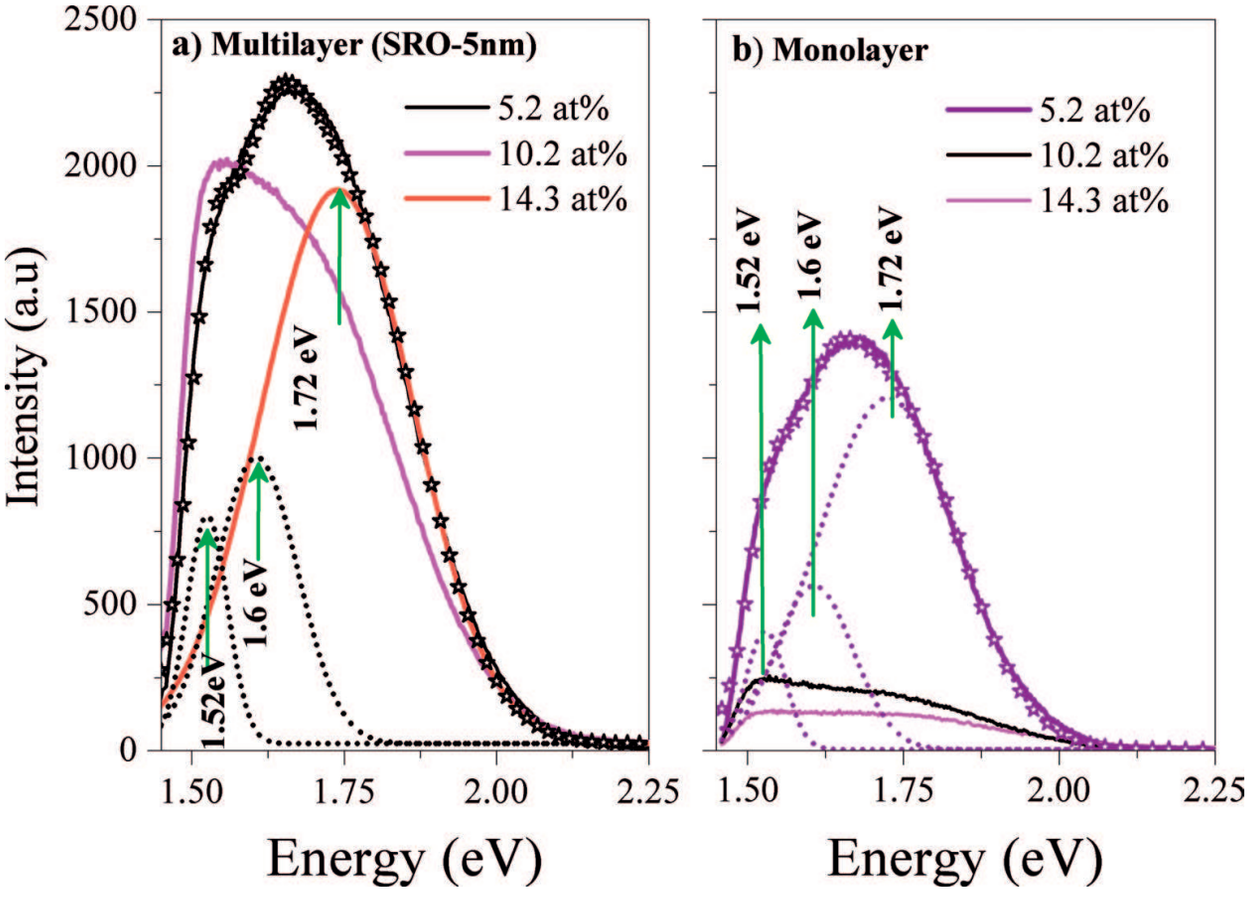

Figure 9. PL spectra of (b) SRO/SiO_2 MLs (SRO-5 nm) with 5.2, 10.2, and 14.3 at.% of Si-excess thermally annealed at 1100°C and (a) SRO monolayers. From Coyopol et al. [28].

most intense photoluminescence is achieved using SRO layers with 5 nm thick and 14 at.% of Si-excess. Such effect is important for the design of electroluminescent devices, particularly for supplying low voltages, since a large number of Si-NCs are generated as Si-excess increases.

The effect of confining Si-NCs in the SRO/SiO_2 MLs is to obtain nanocrystals sizes <3 nm due to the high stress, result in Si=O defects formation. Regarding the presence of Si-NCs and their PL properties, Wolkin et al. suggested that light emission in red-orange region originates from Si=O bonds, where oxidation can stabilize the energy position of the PL peak (~1.5–1.7 eV) from small Si-NCs (<3 nm) [31]. The model of Si=O bonds has been also used to explain the PL emission in connection to Si-NCs in a SiO_2 matrix [32]. It was suggested later that the light-emitting centers can be stabilized not only at Si-NCs surface but also in a disordered network [33], which could be promoted from the phase separation of Si and SiO_2. The emission of the Si=O defect is around 1.5–2.1 eV and it strongly affect the PL intensity when the nanocrystal size is below 3 nm [31].

7. Si-NCs in SRO monolayer and SRO/SiO_2 MLs

The formation of Si-NCs in SRO monolayers and SRO/SiO_2 multilayers was demonstrated by HRTEM analysis [25, 28]. A reduction in nanocrystal size in SRO/SiO_2 MLs respect to SRO

monolayers is shown in **Figure 10a**. In both, SRO/SiO_2 MLs and SRO monolayers, an increase in the average nanocrystal size is observed as the Si-excess increases. However, in the ML structures, the Si-NCs tend to be confined due to the stress exerted by the SiO_x matrix, so that the average nanocrystal size decreases in the MLs compared to the SRO monolayers with the same Si-excess. The increase in size of the Si-NCs according to the Si-excess is expected due to high Si content leads an enhanced in the agglomeration of Si clusters after thermal annealing. It can be deduced that a reduction in Si-NCs size below 3 nm promotes a high PL emission in both SRO monolayers and SRO/SiO_2 multilayers. Recent studies about SRO films confined by two SiO_2 layers have shown that Si atoms in excess from the SRO films mainly diffuse toward the center of the SRO layer, enhancing the Si atom aggregation and thus the Si-NCs formation [8]. Nevertheless, as observed in the XPS depth profile from this work, the Si-excess in the SRO films from SRO/SiO_2 MLs reduces as compared to SRO monolayers. This effect is related with the Si-diffusion from the SRO films toward the SiO_2 layer making them silicon rich instead of stoichiometric films. This Si-diffusion produces three important effects: (i) the Si-NCs formation near the edge of the SRO-SiO_2 interfaces, (ii) the reduction of the Si-NCs size as compared to SRO monolayers and (iii) and as a consequence, the increased Si-NCs density and improved PL intensity.

The phenomenon of light emission in SRO monolayers can be attributed to the presence and complete activation of Si=O defects especially in SRO films with 5.2 at.% where the average

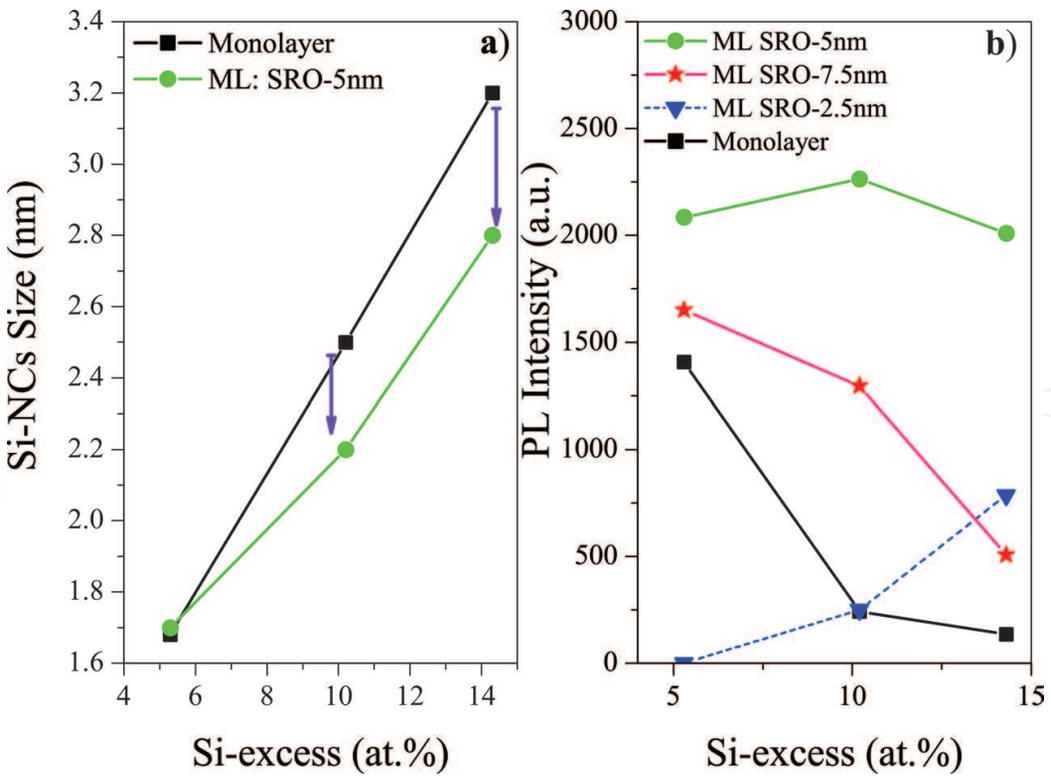

Figure 10. (a) Si nanocrystal size and (b) PL intensity in SRO monolayers and SRO/SiO_2 MLs as a function of Si-excess. From Coyopol et al. [28].

Si-NC size is about 1.68 ± 0.2 nm, as reported in other work [25]. In SRO/SiO_2 MLs, Si-NCs with diameters below 3 nm are necessary to obtain the activation of the Si=O luminescence centers. Therefore, SRO/SiO_2 MLs with SRO-5 nm where Si-NC sizes of about 1.7 ± 0.1, 2.1 ± 0.08 and 2.8 ± 0.09 nm were obtained with Si-excess of 5.2, 10.2 and 14.9 at.%, respectively [28]. The PL intensity for multilayers with SRO-thickness of 5 nm remains almost at the same order as the Si-excess increases, as shown in **Figure 10b**. However, the PL intensity of SRO/SiO_2 MLs with SRO-2.5 nm and SRO-7.5 nm and SRO monolayers decreases as the Si-excess increases. It was observed that the Si-NCs density in SRO/SiO_2 MLs is higher than SRO monolayers produced by a better control of the NCs formation in SRO nanolayers confined between SiO_2 layers. Moreover, Si-NCs with sizes below 3 nm and a large number of Si=O defects are created in SRO/SiO_2 MLs with SRO-thickness of 5 nm. These effects explain the enhanced PL intensity of multilayers making them suitable for the development of silicon-based light sources.

8. Conclusion

In the synthesis of Si-NCs by RF Co-sputtering in SRO monolayers or SRO/SiO_2 multilayers, it is important to consider parameters such as Si-excess, annealing temperature and SRO-thickness layer for SRO/SiO_2 MLs design. These parameters are important for the obtaining of a high emission either in SRO monolayers or SRO/SiO_2 MLs. It can be deduced that a high emission in both; SRO monolayers and SRO MLs is obtained for a medium Si-excess (5.2 at%). However, an important parameter to consider is the Si nanocrystal size. That is, while synthesis of Si-NCs is below 3 nm, a complete activation of Si=O defects are guaranteed. In this way it is possible to obtain a high emission in multilayers with a high Si content. For MLs where the intermediate SRO layer is 5 nm and Si-excess of 14.3 at%, a high emission is obtained due to the confinement of nanocrystals less than 3 nm. Such effect is important for the design of electroluminescent devices, particularly for supplying low voltages, since a large number of Si-NCs are generated as Si-excess increases.

Acknowledgements

Authors want to thank Oscar Solís, Cesar Leyva and Luis Gerardo Silva from CIMAV for the FIB preparation, TEM and XPS measurements, respectively. A. Morales Sánchez acknowledges the support received from CONACYT-CB #180992 and CONACYT-Scientific Infrastructure #269359.

Conflict of interest

There is no conflict of interest with the other authors.

Author details

Antonio Coyopol-Solis[1]*, Tomás Díaz-Becerril[1], Godofredo García-Salgado[1], Santiago A. Cabañas-Tay[2], Liliana Palacios-Huerta[3] and Alfredo Morales-Sánchez[2]

*Address all correspondence to: acoyopol@gmail.com

1 Research Center on Semiconductor Devices (CIDS), Sciences Institute, BUAP, Puebla, México

2 Advanced Materials Research Center (CIMAV), Monterrey-PIIT, Apodaca, Nuevo León, México

3 National Institute of Astrophysics, Optics and Electronics, INAOE, Puebla, México

References

[1] Tseng C-K, Lee M-CM, Hung H-W, Huang J-R, Lee K-Y, Shieh J-M, Lin G-R. Silicon-nanocrystal resonant-cavity light emitting devices for color tailoring. Journal of Applied Physics. 2012;**111**(7):074512. DOI: 10.1063/1.3702793

[2] Zhiping Z, Bing Y, Jurgen M. On-chip light sources for silicon photonics. Light: Science & Applications. 2015;**4**:e358. DOI: 10.1038/lsa.2015.131

[3] Berencén Y, Illera S, Rebohle L, Ramírez JM, Wutzler R, Cirera A, Hiller D, Rodríguez JA, Skorupa W, Garrido B. Luminescence mechanism for Er^{3+} ions in a silicon-rich nitride host under electrical pumping. Journal of Physics D: Applied Physics. 2016;**49**(8):085106. DOI: 10.1088/0022-3727/49/8/085106

[4] Shih C-F, Hsiao C-Y, Su K-W. Enhanced white photoluminescence in silicon-rich oxide/SiO_2 superlattices by low-energy ion-beam treatment. Optics Express. 2013;**21**(13):15888-15895. DOI: 10.1364/OE.21.015888

[5] Vlasukova LA, Komarov FF, Parkhomenko IN, Milchanin OV, Makhavikou MA, Mudryi AV, Żuk J, Kopychiński P, Togambayeva AK. Visible photoluminescence of non-stoichiometric silicon nitride films: The effect of annealing temperature and atmosphere. Journal of Applied Spectroscopy. 2015;**82**(3):386-389. DOI: 10.1007/s10812-015-0117-9

[6] Han PG, Ma ZY, Wang ZB, Zhang X. Photoluminescence from intermediate phase silicon structure and nanocrystalline silicon in plasma enhanced chemical vapor deposition grown $Si/SiO_{(2)}$ multilayers. Nanotechnology. 2008;**19**(32):325708. DOI: 10.1088/0957-4484/19/32/325708

[7] Kim KJ, Moon DW, Hong S-H, Choi S-H, Yang M-S, Jhe J-H, Shin JH. In situ characterization of stoichiometry for the buried SiOx layers in $SiOx/SiO_2$ superlattices and the effect on the photoluminescence property. Thin Solid Films. 2005;**478**:21-24

[8] Yoon JH. Enhanced light emission from Si nanocrystals produced using $SiOx/SiO_2$ multilayered silicon-rich oxides. Applied Surface Science. 2015;**344**:213-216

[9] Lin YH, Wu CL, Pai YH, Lin GR. A 533-nm self-luminescent Si-rich SiNx/SiOx distributed Bragg reflector. Optics Express. 2011;**19**(7):6563-6570

[10] Wu CL, Lin YH, Lin GR. Narrow-Line width and Wavelength-Tunable Red-Light Emission From an Si-Quantum-Dot Embedded Oxynitride Distributed Bragg Reflector. IEEE Journal of Selected Topics in Quantum Electronics. 2012;**18**(6):1643-1649

[11] Alarcon-Salazar J, Zaldívar-Huerta IE, Aceves-Mijares M. Electrical and electroluminescent characterization of nanometric multilayers of SiOX/SiOY obtained by LPCVD including non-normal emission. Journal of Applied Physics. 2016;**119**:215101

[12] Kansawa Y, Hayashi S, Yamamoto K. Raman spectroscopy of Si-rich SiO_2 films: possibility of Si cluster formation. Journal of Physics. Condensed Matter. 1996;**8**:4823

[13] Tomozeiu N, van Hapert JJ, van Faassen EE, Arnoldbik W, Vredenberg AM, Habraken FHPM. Structural properties of a-SiOx layers deposited by reactive sputtering technique. Journal of Optoelectronics and Advanced Materials. 2002;**4**:513

[14] Zacharias M, Yi LX, Heitmann J, Scholz R, Reiche M, Gosele U. Size-controlled Si nanocrystals for photonic and electronic applications. Solid State Phenomena. 2003; **94**:95-104

[15] Kenji I, Masahiko I, Minoru F, Shinji H. Nonlinear optical properties of Si nanocrystals embedded in SiO_2 prepared by a cosputtering method. Journal of Applied Physics. 2009;**105**:093531

[16] Hao XJ, Cho EC, Flynn C, Shen YS, Park SC, Conibeer G, Green MA. Synthesis and characterization of boron-doped Si quantum dots for all-Si quantum dot ándem solar cells. Solar Energy Materials & Solar Cells. 2009;**93**:273-279

[17] Aceves-Mijares M, González-Fernández AA, López-Estopier R, Luna-López JA, Berman-Mendoza D, Morales A, Falcony C, Domínguez C, Murphy-Arteaga R. On the origin of light emission in silicon rich oxide obtained by low-pressure chemical vapor deposition. Journal of Nanomaterials. 2012;**2012**:890701. DOI: 10.1155/2012/890701

[18] Nikitin T, Velagapudi R, Sainio J, Lahtinen J, Räsänen M, Novikov S, Khriachtchev L. Optical and structural properties of SiOx films grown by molecular beam deposition: Effect of the Si concentration and annealing temperature. Journal of Applied Physics. 2012;**112**:094316

[19] Khriachtchev L, Ossicini S, Iacona F, Gourbilleau F. Silicon nanoscale materials: From theoretical simulations to photonic applications. International Journal of Photoenergy. 2012;**2012**:872576. DOI: 10.1155/2012/872576

[20] Morales A, Domínguez C, Barreto J, Riera M, Aceves M, Luna JA, Yu Z, Kiebach R. Spectroscopical analysis of luminescent silicon rich oxide films. Revista Mexicana de Física. 2007;**S53**:279

[21] Dong D, Irene EA, Young DR. Preparation and some properties of chemically vapor-deposited Si-rich SiO_2 and Si_3N_4 Films. Journal of the Electrochemical Society. 1978;**125**:819-823

[22] López-Estopier R, Aceves-Mijares M, Falcony C. Cathodo- and photo-luminescence of silicon rich oxide films obtained by LPCVD. In: Yamamoto N, editor. Cathodoluminescence. Rijeka, Croatia: InTech; 2012. p. 324

[23] Zhang WL, Zhang S, Yang M, Liu Z, Cen ZH, Chen T, Liu D. Electroluminescence of as-sputtered silicon-rich SiOx films. Vaccum. 2010;**84**:1043-1048

[24] Chen XY, Lu YF, Tang LJ, Wu YH, Cho BJ, Xu XJ, Dong JR, Song WD. Annealing and oxidation of silicon oxide films prepared by plasma-enhanced chemical vapor deposition. Journal of Applied Physics. 2005;**97**:014913

[25] Coyopol A, Cardona MA, Diaz-Becerril T, Licea-Jiménez L, Morales-Sánchez A. Silicon excess and thermal annealing effects on structural and optical properties of co-sputtered SRO films. Journal of Luminescence. 2016;**176**:40-46

[26] Yi LX, Heitmann J, Scholz R, Zacharias M. Si rings, Si clusters, and Si nanocrystals—different states of ultrathin SiOx layers. Applied Physics Letters. 2002;**81**:4248

[27] Coyopol A, García-Salgado G, Díaz-Becerril T, Juárez H, Rosendo E, López R, Pacio M, Luna-López JA, Carrillo-López. Optical and structural properties of silicon nanocrystals embedded in SiOx matrix obtained by HWCVD. Journal of Nanomaterials. 2012;**2012**(368268):7

[28] Coyopol A, Cabañas-Tay SA, Díaz-Becerril T, García-Salgado G, Palacios-Huerta L, Morales-Morales F, Morales-Sánchez A. Enhancement of the luminescence by the controlled growth of silicon nanocrystals in SRO/SiO_2 superlattices. Superlattices and Microstructures. 2017;**112**:534-540

[29] Pai PG, Chao SS, Takagi Y, Lucovsky G. Infrared spectroscopic study of SiOx films produced by plasma enhanced chemical vapor deposition. Journal of Vacuum Science & Technology A. 1986;**4**:689-694

[30] Zatryb G, Podhorodecki A, Misiewicz J, Cardin J, Gourbilleau F. Correlation between matrix structural order and compressive stress exerted on silicon nanocrystals embedded in silicon-rich silicon oxide. Nanoscale Research Letters. 2013;**8**:1-7

[31] Wolkin MV, Jorne J, Fauchet PM, Allan G, Delerue C. Electronic states and luminescence in porous silicon quantum dots: The role of oxygen. Physical Review Letters. 1999;**82**:197-200

[32] Khriachtchev L, Novikov S, Lahtinen J. Thermal annealing of Si/SiO_2 materials: Modification of structural and photoluminescence emission properties. Journal of Applied Physics. 2002;**92**:5856-5862

[33] Khriachtchev L, Rasanen M, Novikov S, Pavesi L. Systematic correlation between Raman spectra, photoluminescence intensity, and absorption coefficient of silica layerscontaining Si nanocrystals. Applied Physics Letters. 2004;**85**:1511-1513